

Adaptive robust force control for vehicle active suspensions

Supavut Chantranuwathana¹ and Huei Peng^{2,*},[†]

¹*Department of Mechanical Engineering, Chulalongkorn University, Thailand*

²*Department of Mechanical Engineering, University of Michigan, Ann Arbor, MI 48109-2125, U.S.A.*

SUMMARY

In this paper, the modular adaptive robust control (MARC) technique is applied to design the force loop controller of an electro-hydraulic active suspension system. A key advantage of this modular design approach lies in the fact that the adaptation algorithm can be designed for explicit estimation convergence. The effect of parameter adaptation on force tracking performance can be compensated and thus it is possible to guaranteed certain control performance. Experimental results from a quarter-car active suspension test rig show that when realistic external disturbances and measurement noises exist, the modular design achieves a better estimate than the non-modular ARC design. The improved estimation was found to result in control signals with slightly lower magnitude while maintaining similar tracking performance. Copyright © 2004 John Wiley & Sons, Ltd.

KEY WORDS: adaptive robust control; active suspension; hydraulic actuator

1. INTRODUCTION

The control of active suspension (AS) systems has been enthusiastically studied by many researchers over the last 20 years. Many papers have been published in its control design and performance assessment (see Reference [1] for a comprehensive review). A closer examination of these papers, however, shows that most of these published results were focused on the main-loop design, i.e. on figuring out the active force to be applied, as a function of vehicle states and road disturbance input. Much of the existing literature assumes that the commanded force is produced accurately by an ideal sub-loop control system. Simulation verifications of these main-loop designs were frequently carried out without considering actuator dynamics, or with highly simplified sub-loop dynamics. In reality, actuator dynamics can be quite complicated, and strong interaction between the actuator and the vehicle suspension exists. This is especially true for hydraulic actuators, which remain one of the most viable choices due to their high power-to-weight ratio and low cost. However, hydraulic

*Correspondence to: Huei Peng, Department of Mechanical Engineering, University of Michigan, Ann Arbor, MI 48109-2125, U.S.A.

[†]E-mail: hpeng@umich.edu

actuators also have several adverse attributes: they are non-linear and their force generation capabilities are highly coupled to the vehicle body motions [2]. As a result, little experimental verification on active suspension algorithms has been reported and all of them are confined to low frequency (2–4 Hz) regions [3–5]. Implementation results at higher frequency are desired in order to achieve the full benefit of active suspensions. Specifically, since the vehicle wheel-hop mode is usually around 10 Hz, it is desirable to achieve good force tracking results up to at least 10 Hz.

To help realize the vast number of prior research results on main-loop control designs, several recent works were focused on the sub-loop (force-tracking) control problem. That is, how to design a sub-loop controller to achieve the desired force commanded by the main-loop controller accurately, using a hydraulic actuator. Different approaches have been proposed, and those using linear actuator models (e.g. References [6, 7]) have not found satisfactory results in experiments. When non-linear control algorithms were applied, good force tracking results up to 2 Hz were reported in References [3, 5]. Most of these recent papers emphasize the importance of dealing with uncertainties, because of the fact that parameters may vary significantly in hydraulic systems.

To deal with these uncertainties, robust control [5, 8] and adaptive control [3, 9, 10] techniques have been applied to active suspension applications. The sliding mode control [5, 8] has a significant drawback resulting from the switching at the sliding surface of the control law. In practice, imperfection in control devices and delays often leads to chattering. In AS applications that use hydraulic actuators, chattering degrades performance and may cause instability due to the high-frequency resonance of the fluid column in the actuator. A smoothed version of the controller may be used, however tracking performance is usually significantly compromised. On the other hand, adaptive techniques usually require modifications to guarantee boundedness of the estimates. These make them difficult to guarantee transient tracking accuracy, and asymptotic tracking may be lost even when external disturbances do not exist.

The adaptive robust control (ARC) technique [11] was developed recently to combine the benefits of robust and adaptive control methods while avoiding their drawbacks. More specifically, the main goals of the ARC technique are to achieve guaranteed steady state and transient tracking accuracy (properties of deterministic robust controls) and asymptotic tracking at the absence of disturbances without relying on discontinuous switching or infinite control gains (property of adaptive controls). It is found from our experience, however, that the adaptation algorithm of the original ARC technique does not perform well when significant external disturbances exist. In our laboratory, the estimated parameters usually diverge toward the upper or lower bound which commonly causes higher-than-necessary control gains, or even instability. In this paper, we present a modular ARC technique recently proposed by the authors [12, 13]. The adaptation law is designed specifically for parameter convergence, and proven estimation schemes such as least-square update laws can be used. The new update law was found to be more accurate than the one proposed in the original ARC algorithm, and the control gains are usually reduced.

The remainder of this paper is organized as follows: The model of a quarter-car suspension, including the hydraulic actuation system, is presented in Section 2. Both the force-tracking controller and the main-loop controller used in this work are presented in Section 3. The experimental set-ups and test results are shown in Section 4. Finally, summary and conclusions are given in Section 5.

2. MODELLING

The active suspension system can be divided into two parts: the quarter-car suspension and the hydraulic actuator. These two parts are presented separately in the following two subsections.

2.1. Suspension model

It is widely accepted that a quarter-car model is adequate to study the trade-offs among the three suspension performance goals: ride quality, road holding and suspension packaging. For a quarter-car suspension, vehicle roll and pitch motions are ignored and the only degrees of freedom included are the vertical motions of the sprung mass and the unsprung mass. A lumped and linearized quarter-car suspension model is shown in Figure 1.

In Figure 1, m_s and m_{us} represent the vehicle sprung mass ($\frac{1}{4}$ of the body mass) and the unsprung mass, respectively. k_s and c_s are the stiffness and damping coefficients of the vehicle suspension, k_{us} and c_{us} are the tire stiffness and damping coefficients. x_c , x_w and x_r denote the displacements of the vehicle body, the wheel and the road, respectively. F_a represents the extending force exerted by a hydraulic actuator, both on m_s and m_{us} . It is straightforward to obtain the dynamic equations from the Newton's law:

$$\ddot{x}_c = \frac{1}{m_s}(k_s(x_w - x_c) + c_s(\dot{x}_w - \dot{x}_c) + F_a) \quad (1)$$

$$\ddot{x}_w = \frac{1}{m_{us}}(-k_s(x_w - x_c) - c_s(\dot{x}_w - \dot{x}_c) - F_a + k_{us}(x_r - x_w) + c_{us}(\dot{x}_r - \dot{x}_w)) \quad (2)$$

These two equations can be rewritten in the state space form as

$$\begin{aligned} \dot{X} &= AX + BF_a + G\dot{x}_r \\ Y &= CX + DF_a \end{aligned} \quad (3)$$

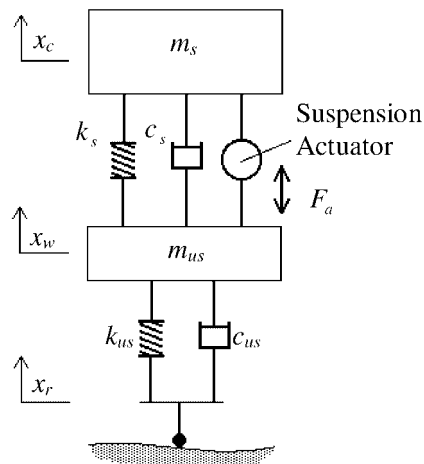


Figure 1. Linear quarter-car suspension model.

where $X = [x_r - x_w, \dot{x}_w, x_w - x_c, \dot{x}_c]^T$. This quarter-car model can be found in numerous publications (e.g. Reference [1]) and thus the details are omitted here. Note that the parameter values are lumped equivalent values combining effects of all suspension components (e.g. bushings) and geometrical characteristics (e.g. tilting angles). It is well known, however, that the lumped model is an accurate approximation and has been widely used in control designs and analyses.

2.2. Actuator model

Figure 2 shows a schematic diagram of an electronically controlled hydraulic actuator. In this figure, P_s is the hydraulic supply pressure and P_r (≈ 0) is the return pressure. x_{sp} is the spool valve displacement, P_u and P_l are the fluid pressures in the upper and lower cylinder chambers of the actuator. $x'_w - x'_c$ is the hydraulic piston displacement which, due to the inclination of the suspension, is approximately equal to $k_{as}(x_w - x_c)$ where k_{as} is a constant. When differences between P_u and P_l exist, the hydraulic cylinder extends or compresses.

Assuming that changes in pressures from their equilibrium values in both sides of the hydraulic cylinder are about the same in magnitude and that the servo-valve dynamics are negligible, a simplified force model can be obtained [8]

$$\dot{F}_a = \beta \left[k_1(\dot{x}_w - \dot{x}_c) - k_2 F_a + k_3 x_{sp} \sqrt{P_s - \text{sgn}(x_{sp}) F_a / A_p} \right] \quad (4)$$

where β is the fluid bulk modulus, $k_1 \equiv k_{as} A_p^2 / V$, $k_{as} \equiv (x'_w - x'_c) / (x_w - x_c)$, A_p is the piston area, V is the total volume of the cylinder chamber, $k_2 \equiv k_p / 2V$, k_p is a damping coefficient, $k_3 \equiv A_p k_{xd} / \sqrt{2} V$, k_{xd} is the orifice flow coefficient and x_{sp} (the spool valve position) is the control input.

3. CONTROLLER DESIGN

The active suspension problem studied in this paper is a disturbance (road undulation) rejection problem. The goal is to achieve good ride quality, road holding and suspension packaging.

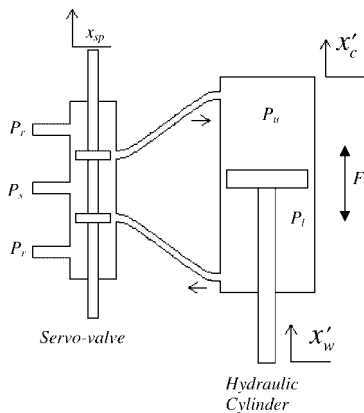


Figure 2. Components of an electro-hydraulic actuator.

More specifically, reduced magnitude in \ddot{x}_c , $x_r - x_w$ and $x_w - x_c$. The control architecture we are using consists of two parts: a force-loop (sub-loop) controller and a main-loop controller as shown in Figure 3. As stated earlier, the main focus of this paper is on the design of the force-loop controller. Two design methods will be used: the original ARC, and a modular ARC design technique. The force-loop controllers are assumed to be working with a main-loop controller, which is designed based on the popular linear quadratic (LQ) design method. A brief discussion of the LQ-based main-loop designs is given in Section 3.1 below.

It is important to note here that the two-loop design approach does not always guarantee the stability of the combined system. We are simply designing a ‘better’ sub-loop controller in this paper. After this is done, the performance limitation of the sub-loop should be considered in the revised main-loop design, which does not make the unrealistic assumption of an infinite-bandwidth sub-loop. This re-design of the main-loop is beyond the scope of this paper.

3.1. Main-loop controller

The LQ and linear quadratic Gaussian (LQG) techniques are the most popular main-loop design approaches because trade-offs among multiple objectives (ride quality, road holding, packaging, etc.) can be included naturally and systematically. By assuming that an ideal force controller is available, the LQ control gains are calculated by minimizing the performance index:

$$J = \int_0^{\infty} (x_r - x_w)^2 + r_1(x_w - x_c)^2 + r_2\ddot{x}_c^2 + r_3F_a^2 dt \quad (5)$$

where r_i are constant weighting factors. The first three terms in the cost function represent three design objectives: road holding, packaging and ride comfort. Using the plant model (Equation (3)) with the parameters shown in Table I, the cost function in Equation (5) and weights $r_1 = 0$, $r_2 = 1 \times 10^{-6}$, $r_3 = 1.3 \times 10^{-12}$, we obtain the LQ gains $[7.074 \times 10^4, -1.192 \times 10^3, 4.876 \times 10^3, 4.854 \times 10^4]$, which are used throughout this work. The closed-loop transfer functions for ride and handling are shown in Figures 4(a) and 4(b), respectively.

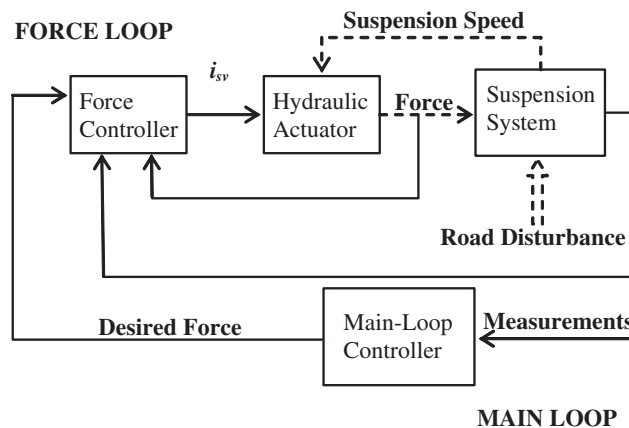


Figure 3. Controller architecture.

Table I. Suspension system parameters.

m_s	285 kg	τ	0.0046 s
m_{us}	40.8 kg	A_p	0.0011 m ²
c_s	535 N/m/s	K_{xd}	0.0012 m ³ /s/N ^{1/2}
c_{us}	747 N/m/s	V	1.16e-4 m ²
k_s	17756 N/m	β	4.4e7 N/m ²
k_{us}	190125 N/m	K_{sv}	0.0157 m/A
P_s	1000 psi	k_f	10000 N/m/s
k_{as}	0.7	k_p	0

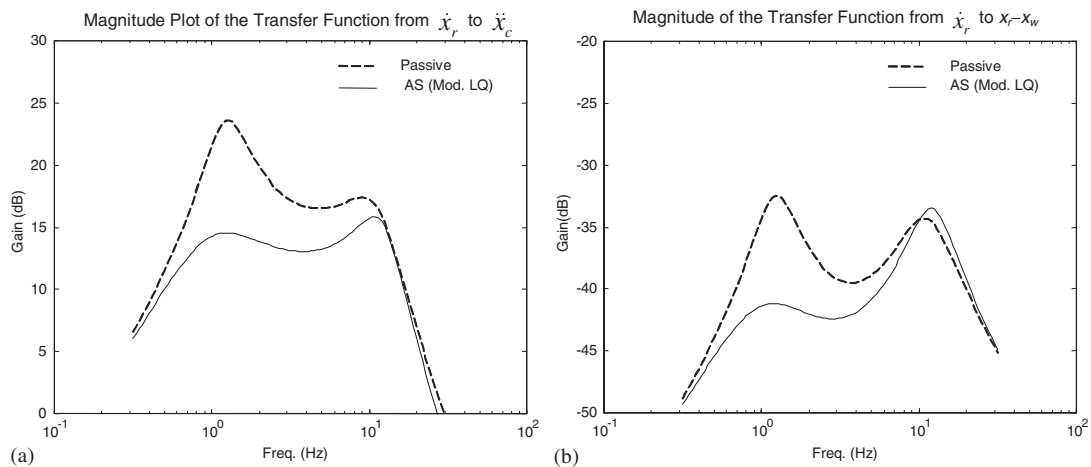


Figure 4. Frequency response of the LQ controlled AS.

For the LQG controller, the LQ gains described above are used with a Kalman-filter to obtain state estimates. It was assumed that the sprung mass acceleration (\ddot{x}_c) and the unsprung mass acceleration (\ddot{x}_w) measurements are available in addition to the suspension stroke. In other words, the output vector is assumed to be $Y = [x_w - x_c, \ddot{x}_w, \ddot{x}_c]$. We use these three measurements because of two reasons. First, it is known that an LQG controller with only suspension stroke measurement is not robust enough [14]. Secondly, accelerometers are cheap and readily available. The disturbance (Q) and measurement noise (R) covariance matrices used are

$$Q = \begin{bmatrix} 1 & 2 & 0 & 0 \\ 2 & 18 & 0 & 0 \\ 0 & 0 & 0.01 & 0 \\ 0 & 0 & 0 & 0.5 \end{bmatrix} \quad \text{and} \quad R = \begin{bmatrix} 1.2 \times 10^{-4} & 0 & 0 \\ 0 & 0.2 & 0 \\ 0 & 0 & 0.02 \end{bmatrix}$$

where R was estimated from sensor readings of our test rig. The matrix Q was constructed to reflect the fact that the road excitation is the main source of disturbances. The off-diagonal

terms are caused by the fact that the same road excitation affects the first two states. Using these matrices, the resulting observer gains are

$$L = \begin{bmatrix} 0.115 & 2.22 & 0.267 \\ -8.36 & 2.79 & 29.6 \\ 1.9 & 4.55 \times 10^{-4} & 0.59 \\ 2.29 & -1.58 & 1.96 \end{bmatrix}$$

3.2. Force-loop controllers

The main objective of the force-loop controllers is to track the desired force commanded by the main-loop controller accurately. Owing to the existence of uncertainties (both general and parametric) in the actuator loop, the force loop was designed based on the ARC technique, to achieve superior robust performance. Among all parameters, the lumped bulk modulus β is the most probable to change significantly because of trapped air, flexibility of tubes, leakage, etc. Therefore, β is modelled as an unknown parameter in the ARC problem formulation. The force loop is designed using both the original ARC and the modular ARC techniques.

3.2.1. ARC controller. The force dynamics (Equation (4)) can be simplified to the following equation:

$$\dot{F}_a = \theta_1[k_1(\dot{x}_w - \dot{x}_c) - k_2F_a + k_3u] + d \quad (6)$$

where

$$u = x_{sp} \sqrt{P_s - \text{sgn}(x_{sp})F_a/A_p} \quad (7)$$

is the virtual control signal. $\theta_1 = \beta$ is the main parameter to be adapted, and d represents general uncertainties arising from un-modelled dynamics and disturbances. We assume that $0 < \theta_{1m} < \theta_1 < \theta_{1M}$ and $|d| < d_M$ and all the bounds are known. In addition to the three measurements used by the main-loop controller, $\dot{x}_w - \dot{x}_c$ (suspension deflection rate) is required by the servo-loop.

Equation (6) is similar to the parametric strict-feedback form in which a procedure for designing an ARC controller is available [11]. Hence, a force controller can be designed using the original ARC techniques. Define $V_1 = \frac{1}{2}z_1^2$, where $z_1 \equiv F_a - F_d$, it can be shown (see Appendix B) that if we apply the control law $u = u_{1a} + u_{1s}$, where

$$u_{1a} = \frac{1}{k_3} \left\{ -k_1(\dot{x}_w - \dot{x}_c) + k_2F_a + \frac{1}{\hat{\theta}_{1\pi}} (\dot{F}_d - c_1z_1) \right\} \quad (8)$$

$$u_{1s} = -z_1 \frac{1}{4\theta_{1m}k_3} \left(\frac{1}{\varepsilon_{11}} \Pi_1^2(k_1(\dot{x}_w - \dot{x}_c) - k_2F_a + k_3u_{1a})^2 + \frac{1}{\varepsilon_{12}} d_M^2 \right)$$

and the parameter update law

$$\dot{\hat{\theta}}_1 = \gamma_1 z_1 [k_1(\dot{x}_w - \dot{x}_c) - k_2F_a + k_3u_{1a}] \equiv \gamma_1 \tau_1 \quad (9)$$

then the Lyapunov function converges exponentially to within a neighbourhood of the origin

$$V_1(t) \leq e^{-2c_1 t} V_1(0) + \frac{\varepsilon_{11} + \varepsilon_{12}}{2c_1} \quad (10)$$

Equation (8) shows that the control law is divided into the adaptive part (u_{1a}) and the robust stability part (u_{1s}). $\hat{\theta}_1$ is the estimate of θ_1 , $\hat{\theta}_{1\pi} \equiv \pi(\hat{\theta}_1)$ is the projected estimate of θ_1 , where $\pi(\cdot)$ is a bounded, smooth, non-decreasing function such that $\pi(\hat{\theta}_1) = \hat{\theta}_1$ when $\hat{\theta}_1 \in [\theta_{1m}, \theta_{1M}]$ and $|\theta_1 - \hat{\theta}_{1\pi}| < \Pi_1$, a known positive constant. F_d is the bounded desired force which is assumed to have a bounded derivative. c_1, ε_{11} and ε_{12} are positive gains.

From Equation (10), it is clear that F_a is bounded whenever F_d is bounded. Furthermore, when the disturbance d is zero, asymptotic tracking can be verified by using the Lyapunov candidate

$$V_2 = \frac{1}{2}z_1^2 + \frac{1}{\gamma_1} \int_0^{\tilde{\theta}_1} (\theta_1 - \pi(\theta_1 - v)) dv$$

where $\tilde{\theta}_1 \equiv \theta_1 - \hat{\theta}_1$. It can be shown that $\dot{V}_2 \leq -c_1 z_1^2$ by using the fact $z_1 u_{1s} \leq 0$. This implies that z_1 converges to zero [11]. Finally, the actual control signal x_{sp} can be computed from Equation (7) by using the virtual control signal u .

3.2.2. Modular ARC controller. In the modular ARC design, the controller is decomposed into a control module and an identifier module—an indirect adaptive control approach. The main goal is to add flexibility to the identifier design without changing the properties of the ARC techniques. This technique has been illustrated in another paper [13] and is also available in Reference [12]. Details are thus omitted here.

The key reason why modularization works is that the effects of the identifier module are dominated rather than cancelled as in the original ARC design. The effects of both estimation error and adaptation rate are included in the control law design. For the hydraulic control problem studied in this paper, the adaptation rate does not affect the dynamics of the plant. As a result, the MARC control law is identical to the original ARC controller. This allows us to compare the performance of the identifiers more easily.

The identification module to be described below is based on a swapping identifier for non-linear systems without general uncertainties [15]. To handle general uncertainties in the ARC formulation, several modifications are required. By combining Equations (6) and (8) and writing in terms of z_1 ($\equiv F_a - F_d$), we obtain

$$\dot{z}_1 = A_z z_1 + \tilde{\theta}_{1\pi} w_1 + d \quad (11)$$

where

$$A_z \equiv -c_1 - \hat{\theta}_{1\pi} k_3 s_1, \quad s_1 = \frac{1}{4\theta_{1m} k_3} \left(\frac{1}{\varepsilon_{11}} \Pi_1^2 (k_1(\dot{x}_w - \dot{x}_c) - k_2 F_a + k_3 u_{1a})^2 + \frac{1}{\varepsilon_{12}} d_M^2 \right),$$

$$\tilde{\theta}_{1\pi} = \theta_1 - \hat{\theta}_{1\pi} \quad \text{and} \quad w_1 = k_1(\dot{x}_w - \dot{x}_c) - k_2 F_a + k_3 u$$

Define two filters

$$\dot{\Omega} = A_z \Omega + w_1, \quad \Omega(t_0) = 0 \quad (12)$$

$$\dot{\Omega}_0 = A_z \Omega_0 + w_1 \hat{\theta}_{1\pi}, \quad \Omega_0(t_0) = -z_1(t_0) \quad (13)$$

it can be shown that

$$e_1 = \Omega \tilde{\theta}_1 + \tilde{e}_1 \quad (14)$$

where $e_1 \equiv z_1 - \Omega \hat{\theta}_1 + \Omega_0$ and

$$\dot{\tilde{e}}_1 = A_z \tilde{e}_1 + d, \quad \tilde{e}_1(t_0) = 0 \quad (15)$$

By using the filters shown in Equations (12) and (13), Equation (6) is replaced by the static equation shown in Equation (14). Since \tilde{e}_1 converges to zero exponentially after finite time when $d = 0$, Equation (14) can be used to design an update law for $\hat{\theta}_1$. To guarantee boundedness of $\hat{\theta}_1$, the update law is selected to be

$$\dot{\hat{\theta}}_1 = P_1 \{ \mu(\hat{\theta}_1) + \Theta(\Omega e_1) \} \quad (16)$$

$$\dot{P}_1 = -P_1^2 \Omega^2 \phi(\Omega e_1), \quad P_1(t_0) > 0 \quad (17)$$

where

$$\mu(\hat{\theta}_1) = \begin{cases} (\theta_{1m} - \hat{\theta}_1), & \hat{\theta}_1 < \theta_{1m} \\ 0, & \theta_{1m} \leq \hat{\theta}_1 \leq \theta_{1M} \\ -(\hat{\theta}_1 - \theta_{1M}), & \hat{\theta}_1 > \theta_{1M} \end{cases}, \quad \Theta(x) = \begin{cases} x, & |x| \leq m_1 \\ m_1 \frac{x}{|x|}, & |x| > m_1 \end{cases}$$

m_1 is an arbitrary positive constant, P_1 is a covariance matrix, and

$$\phi(x) = \begin{cases} m_1/|x| & \text{when } |x| > m_1 \\ 1 & \text{otherwise} \end{cases}$$

The main purpose of function $\Theta(\cdot)$ is to keep the vector Ωe_1 bounded without changing its direction. When combined with $\mu(\cdot)$, these two functions keep the estimate $\hat{\theta}_1$ bounded. In addition, the estimate can be kept positive and away from zero by adjusting m_1 to ensure finite control signals. With these filters and adaptation rules, all states of the identifier module are bounded. Furthermore, output asymptotic tracking is obtained when $d \equiv 0$ (proof is shown in Appendix C). In other words, the desirable properties of the original ARC controller are preserved.

3.2.3. Command signal filtering. Both the ARC and MARC control laws require the derivative of desired force \dot{F}_d (see Equation (8)). This can be obtained by introducing a command signal filter as outlined in Reference [11]. This filter also allows the bounds of the tracking error to be adjusted independently from the initial conditions of the system, which is important for higher-order systems. In this paper, the following filter is used:

$$\begin{aligned} \dot{x} &= -a_f x + F_d \\ Y_r &= \begin{bmatrix} 1 \\ -a_f \end{bmatrix} x + \begin{bmatrix} 0 \\ 1 \end{bmatrix} F_d \end{aligned} \quad (18)$$

where $x \in R$, a_f is a positive constant, $Y_r \equiv [F_{df}, \dot{F}_{df}]^T$ and F_{df} is the filtered desired force signal. F_{df} and \dot{F}_{df} are then used in place of F_d and \dot{F}_d in the control laws.

4. EXPERIMENTAL RESULTS

In this section, experimental results are presented to examine the performance of the MARC algorithm. Three types of experiments are presented: force-loop experiments, complete system experiments and parameter estimation experiments. In the force-loop experiments, the main objective is to show performance of the controllers designed in previous sections without including the main-loop controllers. Bode plots of transfer functions from desired force to actual force are used to present the effectiveness of the controller at various frequencies. In the complete system experiments, the performance under integrated main-loop and force-loop controllers is assessed. Bode plots of the transfer functions from road excitation to sprung mass acceleration and tire deflection are used to present the effectiveness of the controller at various frequencies. Finally, the parameter estimation experiments are used to compare the identification accuracy between the modular and the non-modular controller.

In the first two types of experiments, the parameter adaptations were turned off. This makes it possible for us to separately examine the performance of the control law and the identifier performance. It will be shown later in this paper that the identifier performance of ARC and MARC are quite different. So turning on the identifier will complicate the analysis and discussion of the results. For our application, the ARC and the Modular ARC have identical control laws when their parameter adaptations are turned off. Hence, the control results for the first two sets of experiments are the same for ARC and MARC. Note that the estimate of θ_1 was set to a constant value identified by the Modular ARC controller to be shown in Section 4.3.

The University of Michigan active suspension test rig shown in Figure 5 is a quarter car test rig originally built by the Ford Motor Company. The test rig contains two hydraulic actuators:



Figure 5. The quarter car active suspension test rig.

a road actuator and a suspension actuator. The road actuator is used to simulate road excitation while the suspension actuator is controlled to attenuate the body motions due to the road disturbance. A 15 hp, 20 gpm hydraulic pump running at 1000 psi supplies power to the actuators. Two hydraulic accumulators were installed along the supply line. Three linear variable differential transformers (LVDTs) and two linear velocity transducers (LVTs) are used to measure road displacement, wheel displacement, vehicle body displacement, wheel speed and vehicle body speed, respectively. Two accelerometers were installed to measure the vehicle body acceleration and the wheel acceleration. A force sensor is also available to measure the suspension actuator force. A 120 MHz Pentium computer, an AC-100 DSP board and MATRIXx software are used to facilitate controller implementations.

4.1. Force-loop experiments

For this set of experiments, the main objective is to examine how well the actual force follows the desired force. As stated in Section 1, existing experimental results are limited to 3 Hz or below, but it is desired to achieve 10 Hz or higher. The control parameters used are given in Appendix A.1. Figures 6 and 7 show the force tracking results at 5 and 10 Hz, respectively. In Figure 8, the force tracking results at various frequencies are presented. At each frequency, the response, which is not purely sinusoidal, is replaced by a least-square sinusoidal equivalent. A PD controller is also presented in this plot as a benchmark. The PD control gains are “optimal” obtained through brute-force searching. In this figure, the solid line shows the frequency response of an ideal force controller with 10 Hz bandwidth (simulated). This is expected to be the ideal response of the ARC controller because of the 10 Hz command signal filter.

It can be seen that the bandwidth of the ARC controller is around 8 Hz, and it works quite well up to 10 Hz, which is the range desired for AS applications. On the other hand, the PD

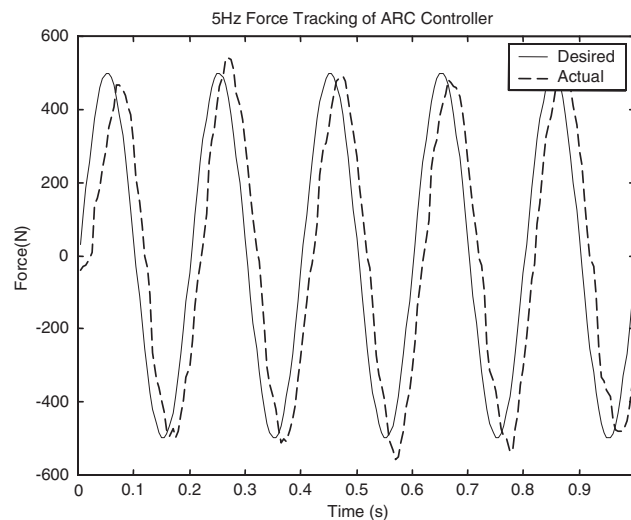


Figure 6. ARC force tracking at 5 Hz.

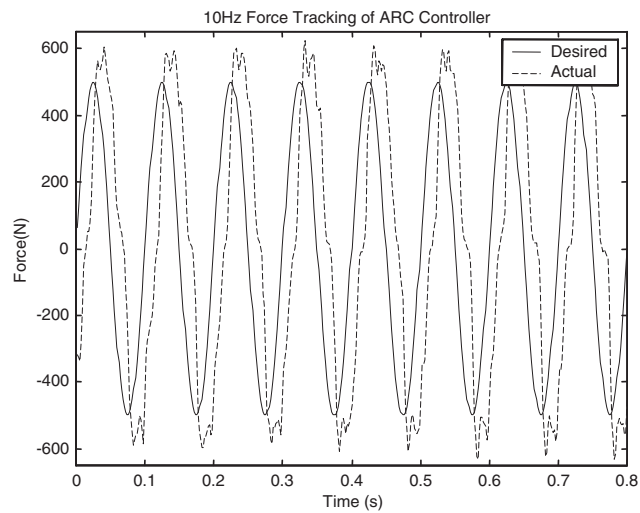


Figure 7. ARC force tracking at 10 Hz.

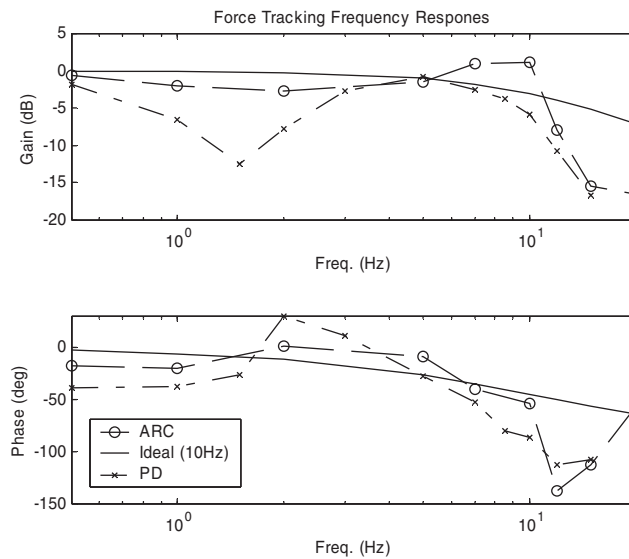


Figure 8. ARC force tracking at various frequencies.

controller performs well only up to 0.5 Hz and between 3 and 5 Hz. Note that, it is possible to improve the performance of the ARC controller. However, we found that most of those controllers will have higher gains and become unstable when combined with the main-loop controller.

The results shown above are qualitatively similar to those in recent papers by Alleyne (e.g. Reference [9]), even though the plants are not the same. In particular, the interaction between

the actuator and the plant results in transfer function zeroes at different frequencies (two zeroes at 4 Hz in Reference [9], and two zeroes at 1 Hz and two zeroes at 10 Hz for this paper).

4.2. Complete system experiments

The performance of the combined inner-outer-loop controllers is presented in this section. Two outer-loop controllers are used: LQ and LQG controllers. An ideal (simulated) force controller with 10 Hz bandwidth will be used as the benchmark. Although the system is non-linear, transfer functions at prescribed input levels will be reported as is commonly used in the literature, e.g. Reference [5]. The transfer functions from \dot{x}_r to \ddot{x}_c and $x_r - x_w$, (representing ride comfort and handling) are used as the main performance indices of the controllers [1]. A controller is said to perform well if its transfer function magnitude is close to that of the closed-loop system with an ideal force controller. The performance of the closed-loop system with PD force-loop controller is also presented for comparison.

The LQ controller, which requires full-state feedback, represents an ideal outer-loop controller. The performance degradation (comparing the LQ-ARC with the simulated LQ-ideal) is likely due to the force-loop controller. The LQG controller represents a more realistic implementation of the outer-loop controller, and thus the performance of LQG-ARC is of interest. The LQG controller is assumed to use information that can be measured cheaply ($x_w - x_c$, \ddot{x}_w , \ddot{x}_c and F_a). On the contrary, the LQ controller requires information that is hard to measure directly, including tire deflection and its rate of change, which makes it impractical for real applications.

The experimental results are shown in Figures 9 and 10. In each figure, the dashed line represents a passive suspension (simulated). Its parameter values are the same as the test rig except that the suspension's damping ratio is changed from 12 to 35% for closer representation of a typical passive suspension [16]. This is due to the fact that the pneumatic spring used in our test rig is not meant to work by itself and thus has a lower-than-normal damping. The solid line represents the (simulated) LQ controller with an ideal force-loop controller (10 Hz bandwidth). The closer the experimental results are to this line, the better the controller performance is. In addition, if the experimental results are lower than the dashed line, that means the controller performs better than the passive suspension system. For ride quality, the critical frequency range is 4–8 Hz and for tire deflection, lower frequencies are more important than higher frequencies.

Figure 9 shows that the ARC controller performs very well when combined with the LQ controller. Except for frequencies higher than 10 Hz, the ARC controller's performance is close to that of the ideal force-loop controller (within ± 3 dB). Overall, the LQ-ARC performs better than the passive system up to 10 Hz. It improves ride comfort (smaller \ddot{x}_c) and enhances handling (lower $x_r - x_w$). Figures 9(a) and 9(b) also show that the LQG-ARC controller works essentially as well as the LQ-ARC controller in terms of reducing sprung mass acceleration. However, the LQG-ARC controller has slightly worse tire deflection performance between 3 and 5 Hz. This performance reduction is probably caused by state estimation problems, especially tire deflection and its derivative. Tire deflection is difficult to estimate since it is extremely small and is directly influenced by the road disturbance.

Comparing the results of the LQ/LQG-ARC with the LQ/LQG-PD controller in Figure 10(a) and 10(b), one can see that the performance of the LQ/LQG-PD controller is very poor, especially around intermediate to high frequencies (3–10 Hz). The LQ-PD controller performs better than the passive system only for frequencies up to 2 Hz.

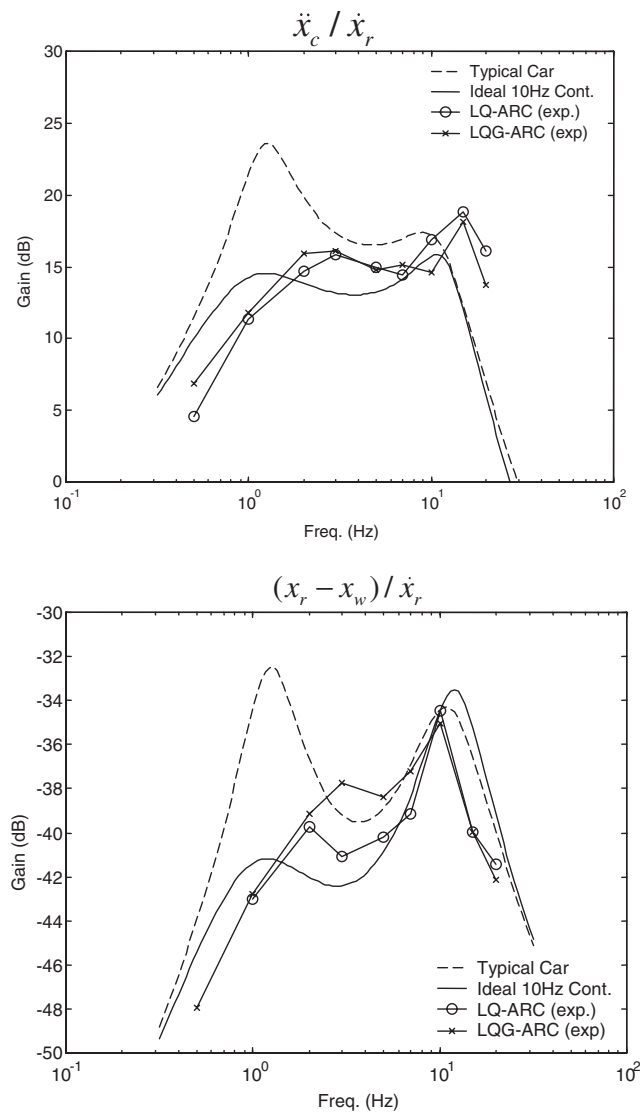


Figure 9. LQ/LQG-ARC transfer function gains (\dot{x}_r to \ddot{x}_c and \dot{x}_r to $x_r - x_w$).

4.3. Parameter estimation experiments

In this section, the performance of the modular ARC in identifying unknown parameter (θ_1) is verified experimentally. The parameters of the controllers are given in Appendix A.2. The experiments simulate the actual working conditions of a complete AS system (LQ-MARC). Realistic road excitations were generated by passing a Gaussian white noise signal through a first-order low-pass filter (cut-off at 10 Hz). The signal's power was adjusted such that the resulting power spectral density around 1–10 Hz region is close to that of a medium-roughness highway [16].

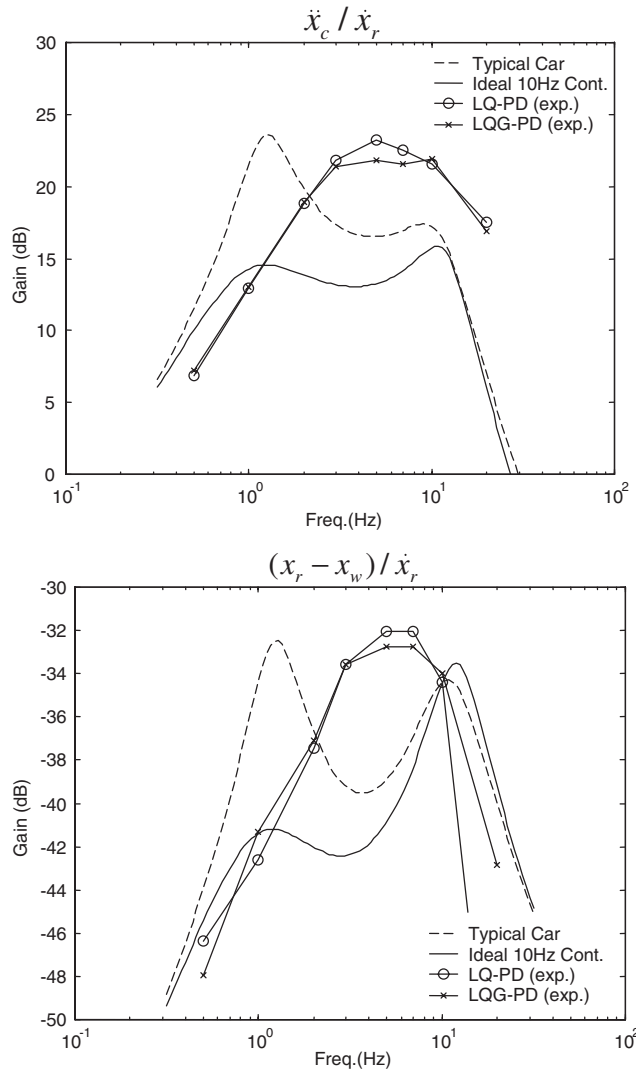


Figure 10. LQ/LQG-PD transfer function gains (\dot{x}_r to \ddot{x}_c and \dot{x}_r to $x_r - x_w$).

From our experience, it was found that the estimation accuracy can be significantly improved by slightly modifying the modular ARC controller presented in Section 3. First, it was observed that the force between the sprung mass and the unsprung mass is $F_m = F_a + k_f(\dot{x}_w - \dot{x}_c)$, where the friction is modelled simply as a damper with a constant k_f and F_a is the force resulting from fluid pressures only. As a result, we see that Equation (14) must be changed to

$$e_1 = \Omega^T \tilde{\theta}_1 + \tilde{k}_f(\dot{x}_w - \dot{x}_c) + \tilde{e}_1 \tag{19}$$

where e_1 is calculated using the measured force; i.e. $e_1 = F_m - F_d - \Omega \tilde{\theta}_1 + \Omega_0$, $\tilde{k}_f = k_f - \hat{k}_f$ and \hat{k}_f is an estimate of k_f . Secondly, we added a small constant to the covariance update equation in order to prevent the adaptation from stopping entirely. This is similar to the covariance

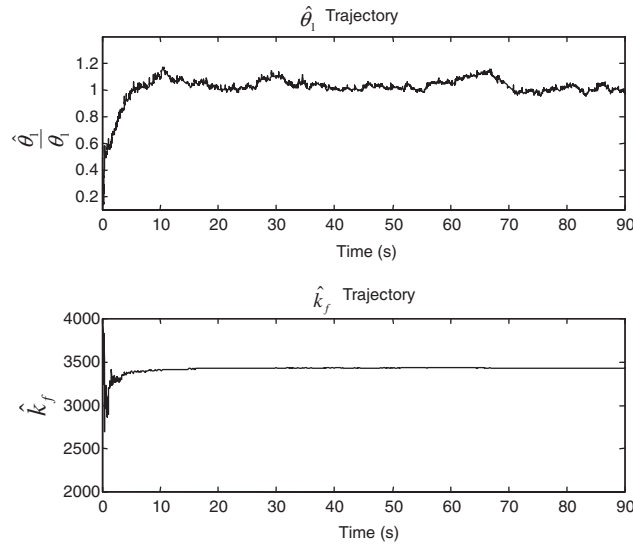


Figure 11. Experimental result of LQ-MARC ($\hat{\theta}_1(t_0) = 0.5\theta_1$).

resetting method but is easier to implement. With these two modifications, the new adaptation rules are

$$\dot{\hat{\theta}}_1 = \gamma_1(P_1 + p_1)(\mu(\hat{\theta}_1) + \Theta(\Omega e_1)) \quad (20)$$

$$\dot{\hat{k}}_f = \gamma_2(P_2 + p_2)(\dot{x}_w - \dot{x}_c)e_1 \quad (21)$$

$$\dot{P}_1 = -P_1^2 \Omega^2 \phi(\Omega e_1) \quad (22)$$

$$\dot{P}_2 = -P_2^2 (\dot{x}_w - \dot{x}_c)^2 \quad (23)$$

Note that the estimate of k_f helps to improve the accuracy of e_1 , and hence the accuracy of the estimate of $\hat{\theta}_1$. We should mention that this friction identification is presented here, rather than earlier, because it is not part of our control scheme. In particular, the friction parameter is identified but not used in the control law. Its existence, however, improved the estimation of the bulk modulus. It is possible to include the friction in the model when designing the control law. However, the controller uses the $\dot{x}_w - \dot{x}_c$ signal which is usually quite noisy.

Figure 11 shows the time trajectories of the estimates of LQ-MARC where $\hat{\theta}_1(t_0) = 0.5\theta_1$. It can be seen that the estimate converges to the neighbourhood of the actual value. The estimate of k_f also converges, but we do not know whether it is close to the real value or not. The same experiment was performed with the original ARC controller (LQ-ARC). It can be seen from Figure 12 that the estimate of θ_1 diverges to the lower limit. We started this experiment at $\hat{\theta}_1(t_0) = 2\theta_1$ because else $\hat{\theta}_1$ will have hit the lower bound right away.

How important is a more accurate parameter estimation? It is commonly accepted that the estimations from a Lyapunov-based adaptation law can grow unbounded in real applications if no extra patches/modifications are applied. It can be seen from Figure 12 that the estimate from

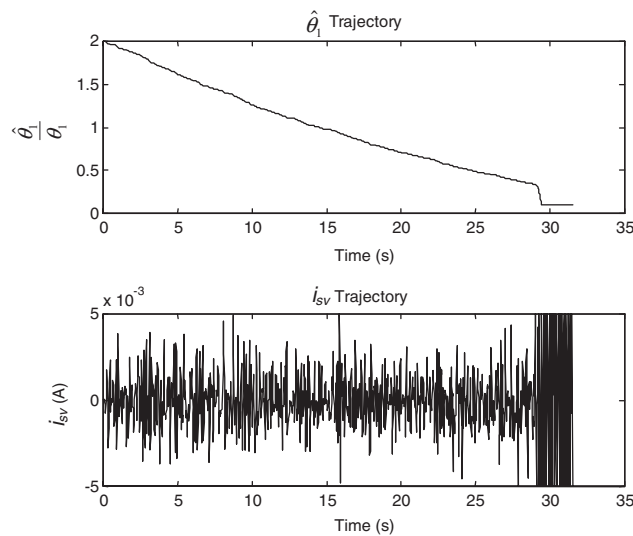


Figure 12. Experimental result of LQ-ARC ($\hat{\theta}_1(t_0) = 2\theta_1$).

the LQ-ARC controller diverges to its lower bound. Since the estimate appears in the denominator of the control law, the ARC controller uses higher gain compared with the MARC controller. As a result, the system may become unstable if the parameter lower bound (θ_{1m}) is too small, as can be seen from Figure 12 ($t > 30$ s). It is important to note that from simulations we found that the estimates from the ARC identifier can be accurate when uncertainties are sufficiently small [8, 9]. For real vehicle applications, however, this requirement may impose additional cost (better sensors) and operational constraints. Therefore, the MARC identification scheme may be more practical.

5. SUMMARY AND CONCLUSION

In this paper, we studied the application of the newly developed modular ARC (MARC) controller [12, 13] to the force control loop of an active suspension system. Experimental results show that the proposed MARC controller performs the force tracking task very well up to about 10 Hz, which is considerably higher than the < 4 Hz results reported in the literature [4, 5]. With the main loop controller, the results show that the controller performs satisfactorily compared to the ideal force controller up to 10 Hz. The MARC controller was found to perform much better than an ‘optimal’ PD controller. The integrated main-loop and sub-loop performance was investigated, and the active suspension outperformed the passive suspension system up to about 10 Hz in terms of ride quality. The tire deflection performance is only improved up to about 2 Hz. Since tire deflection is related to tire lateral/longitudinal force generation, this improvement may be adequate.

Finally, in the parameter identification experiments, the advantages of the modular ARC controller over the original ARC were verified. Experimental results show that the parameter estimation converged in the modular ARC design but diverged in the original ARC design. For

actual implementation in active suspension, the improved estimation is important because smaller control signals could be used.

APPENDIX A: CONTROL PARAMETERS

A.1. Controller parameters for the force tracking experiments and the complete system experiments

$$c_1 = 140, \varepsilon_{11} = \varepsilon_{12} = 15000, d_M = 50, \theta_{1m} = 0.9\theta_1, \theta_{1M} = 1.1\theta_1, \hat{\theta}_1 \equiv 1.1\theta_1 \text{ and } a_f = 62.$$

A.2. Controller parameters for the estimation experiments

$$c_1 = 100, \varepsilon_{11} = \varepsilon_{12} = 80000, d_M = 0, \theta_{1m} = 0.1\theta, \theta_{1M} = 2\theta, k_f(t_0) = 3000, a_f = 62, \gamma_1 = 0.05, \gamma_2 = 800, p_1 = 0.0005, p_2 = 0.01, P_1(t_0) = 1, P_2(t_0) = 1.$$

APPENDIX B: PROPERTIES OF THE ARC FORCE CONTROLLER

B.1. The guaranteed tracking accuracy of the system is provided by Equation (10) which is obtained as follows. Let $V_1 = \frac{1}{2}z_1^2$, using Equations (6) and (8), we have

$$\begin{aligned} \dot{V}_1 &= z_1((\tilde{\theta}_{1\pi} + \hat{\theta}_{1\pi})(k_1(\dot{x}_w - \dot{x}_c) - k_2F_a + k_3u_{1a}) + \theta_1k_3u_{1s} + d - \dot{F}_d) \\ &= -c_1z_1^2 + z_1(\tilde{\theta}_{1\pi}(k_1(\dot{x}_w - \dot{x}_c) - k_2F_a + k_3u_{1a}) + \theta_1k_3u_{1s} + d) \end{aligned}$$

where $\tilde{\theta}_{1\pi} \equiv \theta_1 - \hat{\theta}_{1\pi}$. By the defined u_{1s} and completing the squares, we have

$$\dot{V}_1 \leq -c_1z_1^2 + \varepsilon_{11} + \varepsilon_{12} = -2c_1V_1 + \varepsilon_{11} + \varepsilon_{12}$$

which results in Equation (10).

B.2. The asymptotic tracking property of the system (when $d = 0$) is obtained as follows. Let

$$V_2 = \frac{1}{2}z_1^2 + \frac{1}{\gamma_1} \int_0^{\tilde{\theta}_1} (\theta_1 - \pi(\theta_1 - v)) dv$$

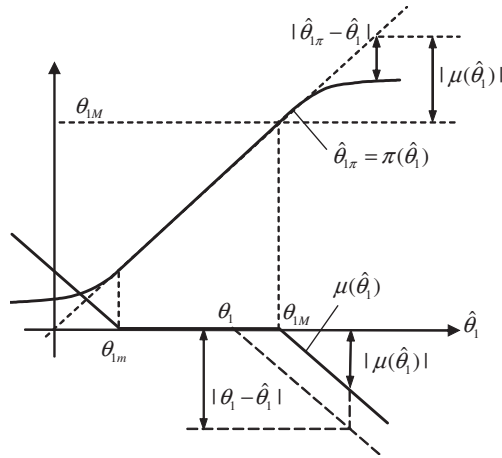
Note that V_2 is positive definite. Differentiate V_2 and note $z_1k_3u_{1s} \leq 0$, we have

$$\begin{aligned} \dot{V}_2 &\leq z_1((\tilde{\theta}_{1\pi} + \hat{\theta}_{1\pi})(k_1(\dot{x}_w - \dot{x}_c) - k_2F_a + k_3u_{1a}) - \dot{F}_d) - \frac{\tilde{\theta}_{1\pi}}{\gamma_1} \dot{\hat{\theta}} \\ &\leq -c_1z_1^2 + z_1\tilde{\theta}_{1\pi}(k_1(\dot{x}_w - \dot{x}_c) - k_2F_a + k_3u_{1a}) - \frac{\tilde{\theta}_{1\pi}}{\gamma_1} \dot{\hat{\theta}} \end{aligned}$$

If we choose $\dot{\hat{\theta}}_1 = \gamma_1 z_1(k_1(\dot{x}_w - \dot{x}_c) - k_2F_a + k_3u_{1a})$, $\dot{V}_2 \leq -c_1z_1^2$, i.e. z_1 converges to zero asymptotically.

APPENDIX C: OUTPUT ASYMPTOTIC TRACKING UNDER $d = 0$

It is obvious that $\hat{\theta}_1$ is positive due to the saturation bounds used in the design of $\Theta(\cdot)$ and $\mu(\cdot)$. From Equation (10), z_1 and F_a are bounded. Therefore, u_{1a}, u_{1s}, Ω and Ω_0 are all bounded. P_1 is bounded because it is positive and non-increasing.

Figure C1. Functions $\pi(\hat{\theta}_1)$ and $\mu(\hat{\theta}_1)$.

Asymptotic tracking when $d \equiv 0$ is obtained as follows. From Equations (14) and (15), \tilde{e}_1 is identically zero. Let $V_3 = (1/2P_1)\tilde{\theta}_1^2$, we have $\dot{V}_3 \leq -\tilde{\theta}_1(\mu(\hat{\theta}_1) + \Theta(\Omega e_1)) + (\tilde{\theta}_1^2/2)\Omega^2\phi$. Using Equation (14) and the fact that $\theta_1\mu(\hat{\theta}_1) \geq \mu^2(\hat{\theta}_1)$ (see Figure C1), we have

$$\dot{V}_3 \leq -\mu^2(\hat{\theta}_1) + \tilde{\theta}_1\Theta(\Omega e_1) + \frac{e_1^2}{2}\phi \quad (\text{C1})$$

When $\Omega e_1 \leq m_1$, we have $\Theta(\Omega e_1) = \Omega e_1$, $\phi = 1$, and Equation (C1) can be written as

$$\dot{V}_3 \leq -\mu^2(\hat{\theta}_1) - \frac{e_1^2}{2} \quad (\text{C2})$$

When $\Omega e_1 > m_1$, $\Theta(\Omega e_1) = \phi_1\Omega e_1$, $\phi = m_1/|\Omega e_1|$ and Equation (C1) becomes

$$\dot{V}_3 \leq -\mu^2(\hat{\theta}_1) - \frac{\phi e_1^2}{2} \quad (\text{C3})$$

In either case, Equation (C.3) holds true. Integrating both side of Equation (C3), we obtain

$$V_3(t_0) - V_3(\infty) \geq \int_{t_0}^{\infty} \mu^2(\hat{\theta}_1) + \int_{t_0}^{\infty} \frac{\phi e_1^2}{2}$$

Since V_3 is positive and non-increasing, $V_3(\infty)$ exists, $\mu(\hat{\theta}_1) \in L_2$. Similarly, $e_1 \in L_2$ since ϕ cannot be arbitrarily close to zero. It follows from Equation (14) that $\Omega\tilde{\theta}_1 \in L_2$ and $\hat{\theta}_1 \in L_2$ since P_1 and Ω are bounded.

Next, we will show that $z_1 \in L_2$. Let $\psi = \Omega_0 - \Omega\hat{\theta}_1$, we have $\dot{\psi} = A_z\psi - \Omega\dot{\hat{\theta}}_1 + w_1(\hat{\theta}_{1\pi} - \hat{\theta}_1)$. Further, $(\hat{\theta}_{1\pi} - \hat{\theta}_1) \in L_2$ since $|\mu(\hat{\theta}_1)| \geq |\hat{\theta}_{1\pi} - \hat{\theta}_1|$ (Figure C1). Since $\Omega\dot{\hat{\theta}}_1 + w_1(\hat{\theta}_{1\pi} - \hat{\theta}_1) \in L_2$ we have $\psi \in L_2$. Using the fact $z_1 = \Omega\theta_1 - (\Omega_0 - \Omega\hat{\theta}_1) - \Omega\hat{\theta}_1 = \Omega^T\tilde{\theta}_1 - \psi$, $z_1 \in L_2$. Finally, from Equation (11), by noting the boundedness of all signals established earlier, \dot{z}_1 is bounded. Using the Barbalat's Lemma, it follows that $z_1 \rightarrow 0$.

REFERENCES

1. Hrovat D. Survey of advanced suspension developments and related optimal control applications. *Automatica* 1997; **33**(10):1781–1817.
2. Alleyne A, Liu R. On the limitations of force tracking control for hydraulic servo systems. *Journal of Dynamic Systems, Measurement and Control, Transactions of the ASME* 1999; **121**(2):184–190.

3. Alleyne A, Hedrick JK. Nonlinear adaptive control of active suspension. *IEEE Transactions on Control Systems Technology* 1995; **3**(1):94–101.
4. Goran MB, Bachrach BI, Smith RE. The design and development of a broad bandwidth active suspension concept car. Total vehicle dynamics-FISITA 1992; *Automotive technology serving society*; **2**:231–252.
5. Rajamani R, Hedrick JK. Performance of active automotive suspensions with hydraulic actuators: theory and experiment. *Proceedings of the American Control Conference*, June 1994: 1214–1218.
6. Engelman GH, Rizzoni G. Including the force generation process in active suspension control formulation. *Proceedings of the 1993 American Control Conference*; 701–705.
7. Strathearn RR. Active suspension design and evaluation using a quarter car test rig. *Master's Thesis*, University of Michigan, 1996.
8. Alleyne A, Neuhaus PD, Hedrick JK. Application of nonlinear control theory to electronically controlled suspensions. *Vehicle System Dynamics* 1993; **22**:309–320.
9. Alleyne A, Liu R. A simplified approach to force control for electro-hydraulic systems. *Control Engineering Practice* 2000; **8**:1347–1356.
10. Kim E. Nonlinear Indirect adaptive control of a quarter car active suspension. *Proceedings of the 1996 IEEE International Conference On Control Applications*. September 1996; 61–66.
11. Yao B, Tomizuka M. Adaptive robust control of SISO nonlinear systems in a semi-strict feedback form. *Automatica* 1997; **33**(5):893–900.
12. Chantranuwathana S. Adaptive robust force control for vehicle active suspensions. *Ph.D.'s Dissertation*, University of Michigan, 2001.
13. Chantranuwathana S, Peng H. Modular adaptive robust control of SISO nonlinear systems in semi-strict feedback form. *International Journal of Robust and Nonlinear Control* 2004; **14**(6).
14. Ulsoy AG, Hrovat D, Tseng T. Stability robustness of LQ and LQG active suspension. *ASME Journal of Dynamic Systems, Measurement, and Control* 1994; **v116**:123–131.
15. Krstic M, Kanellakopoulos I, Kokotovic P. *Nonlinear and Adaptive Control Design*. Wiley: New York, 1995.
16. Gillespie TD. *Fundamentals of Vehicle Dynamics*. Society of Automotive Engineers, Inc.: Pennsylvania, USA.